Identification of Preferred Multimodal Ligand Binding Regions on IgG1 FC using Nuclear Magnetic Resonance and Molecular Dynamics Simulations

Ronak Gudhka[1], Camille Bilodeau[1], Scott McCallum[1], Mark McCoy[2], David Roush[2], Mark Snyder[3], and Steven Cramer[1]

[1]Rensselaer Polytechnic Institute
[2]Merck and Co., Inc.
[3]Bio-Rad Laboratories

July 30, 2020

Abstract

In this study, the binding of multimodal chromatographic ligands to the IgG1 FC domain were studied using nuclear magnetic resonance and molecular dynamics simulations. Nuclear magnetic resonance experiments carried out with chromatographic ligands and a perdeuterated 15N-labeled FC domain indicated that while single mode ion exchange ligands interacted very weakly throughout the FC surface, multimodal ligands interacted with specific clusters of residues with relatively high affinity, forming distinct binding regions on the Fc. The multimodal ligand binding sites on the FC were concentrated in the hinge region and near the interface of the CH2 and CH3 domains. Further, the multimodal binding sites were primarily composed of positively charged, polar and aliphatic residues in these regions, with histidine residues exhibiting some of the strongest binding affinities with the multimodal ligand. Interestingly, comparison of protein surface property data with ligand interaction sites indicated that the patch analysis on FC corroborated molecular level binding information obtained from the nuclear magnetic resonance experiments. Finally, molecular dynamics simulation results were shown to be qualitatively consistent with the nuclear magnetic resonance results and to provide further insights into the binding mechanisms. An important contribution to multimodal ligand-FC binding in these preferred regions was shown to be electrostatic interactions and pi-pi stacking of surface exposed histidines with the ligands. This combined biophysical and simulation approach has provided a deeper molecular level understanding of multimodal ligand-FC interactions and sets the stage for future analyses of even more complex biotherapeutics.

Introduction

A range of multimodal (MM) chromatographic systems have been developed which exhibit enhanced selectivity as compared to single mode interaction resins due to a combination of electrostatic, hydrophobic, aromatic and/or hydrogen bonding interactions within a single ligand (S. C. Burton, Haggarty, & Harding, 1997; Simon Christopher Burton & Harding, 1997; Cramer & Holstein, 2011; Ghose, Hubbard, & Cramer, 2005; Holstein, Parimal, McCallum, & Cramer, 2012; Johansson et al., 2003; Melander, El Rassi, & Horváth, 1989). Further, new prototypes of MM resins that vary in solvent exposure and presentation of functional groups as well as those having differences in linker length and chemistry have been shown to have unique windows of selectivity (Robinson, Snyder, et al., 2018; J. A. Woo et al., 2015; J. Woo, Parimal, Brown, Heden, & Cramer, 2015). The utility of MM chromatography has also been demonstrated for important industrial applications such as the capture of mAbs and related formats (Arakawa, Kita, Sato, & Ejima, 2009; Gagnon et al., 2010; Kaleas, Tripodi, Revelli, Sharma, & Pizarro, 2014; Pezzini et al., 2011) as well as

for challenging polishing steps such as removal of product related variants, fragments and aggregates (Chen et al., 2010; Liu, Ma, Winter, & Bayer, 2010; O'Connor et al., 2017).

In order to design novel chromatographic ligands and to facilitate process development for downstream bioprocessing, a deeper understanding of protein binding regions with chromatographic systems is important. Several groups have contributed to the understanding of protein interactions in single mode interaction systems and some representative examples are presented here. Roush et al. identified patches on rat cytochrome b_5 for interaction with an anion exchange surface using a series of computational and experimental studies (Roush, Gill, & Willson, 1994). Yao et al. investigated the distribution of charges on the surface of cytochrome c and its variants and explained the retention behavior on cation exchange systems (Yao & Lenhoff, 2004). Sun et al. employed a computational approach to predict preferred binding orientations in both cation exchange (CEX) and hydrophobic interaction systems (Sun, Welsh, & Latour, 2005). Dismer et al. utilized a lysine specific fluorescent dye (Cy5) to identify the binding orientation of lysozyme on a cation exchange surface under various mobile phase conditions (Dismer & Hubbuch, 2007; Dismer, Petzold, & Hubbuch, 2008). Our group has previously employed amino acid specific covalent labeling in combination with mass spectrometry (MS) to examine the binding regions of protein libraries generated from lysozyme and cytochrome C in a cation exchange system (Chung, Evans, et al., 2010; Chung, Holstein, et al., 2010). Kittelmann et al. recently developed QSAR models for predicting binding orientation of antibodies on CEX chromatographic surfaces (Kittelmann, Lang, Ottens, & Hubbuch, 2017).

Studies have also been carried out on understanding preferred binding regions of proteins in more complex systems such as hydrophobic charge induction (HCIC) and MM CEX. Zhang et al. performed a series of molecular dynamics (MD) simulations to study the changes in binding orientation of a β- barrel protein on HCIC surface as a function of salt concentration (Zhang, Zhao, & Sun, 2009). Yu et al. employed coarse-grained simulations to investigate the preferred binding orientation of lysozyme on a HCIC surface at different ligand densities under a range of salt concentrations (Yu, Liu, & Zhou, 2015). Our lab has been actively involved in studying the preferred binding regions of small proteins in MM CEX systems by employing protein libraries (Chung, Hou, et al., 2010), MD simulations (Banerjee, Parimal, & Cramer, 2017; Freed, Garde, & Cramer, 2011; Parimal, Garde, & Cramer, 2015, 2017), Atomic Force Microscopy (AFM) (Srinivasan et al., 2017) and Nuclear Magnetic Resonance (NMR) (Chung, Freed, et al., 2010; Holstein, Chung, et al., 2012; Holstein, Parimal, McCallum, & Cramer, 2013; Srinivasan, Parimal, Lopez, McCallum, & Cramer, 2014).

Ligand-induced chemical shift perturbations (CSP) have been widely used to identify binding regions on proteins (Clarkson & Campbell, 2003). The sensitivity of the chemical shifts to changes in the local environment enables the identification of ligand complexation at an atomic level, while also being able to accurately determine the residue level binding affinity (Hong et al., 2009; Lu, Guo, Jin, & Xiao, 2009; Williamson, 2013). Previous work in our group employed 2D heteronuclear single quantum correlation (HSQC) NMR experiments to identify binding sites of single mode and MM CEX ligands on a small model protein, ubiquitin, and its mutants (Chung, Freed, et al., 2010; Holstein, Chung, et al., 2012). NMR was also employed to evaluate the effects of urea on preferred binding regions in MM systems (Holstein et al., 2013). Further, we have employed MM functionalized gold nanoparticles in solution to identify binding regions on ubiquitin using NMR (Srinivasan et al., 2014). We have also employed NMR in concert with MD simulations to obtain more detailed molecular level information on protein interactions in multimodal systems (Holstein, Chung, et al., 2012).

While the understanding of small protein binding in multimodal chromatographic systems is valuable, it is important to extend these studies to more complex and industrially relevant biomolecules. One such protein is the F_C domain, which is highly conserved across a given class of mAbs and which plays an important role in a number of biotherapeutics such as bispecific antibodies and fusion proteins (Shukla, Hubbard, Tressel, Guhan, & Low, 2007). Robinson et al. has examined the domain contributions of mAb binding using a strategic set of chromatographic experiments and shown a shift in domain dominance with pH and resin type (Robinson, Roush, & Cramer, 2018, 2020). Gagnon et al. demonstrated that the binding of the

F_C domain was driven by calcium affinity interactions in hydroxyapatite (HA) chromatography (Gagnon, Cheung, & Yazaki, 2009). Lin et al. employed molecular simulations to identify preferred binding sites of an HCIC ligand (MEP Hypercel) on single-chain F_C fragments (Lin, Tong, Wang, & Yao, 2012). Even though these studies have improved our understanding of F_C binding in MM systems, there is clearly a need to develop a deeper understanding of these interactions at the molecular level.

In the present study, we employ a combination of NMR and molecular simulations to examine the interactions of chromatographic ligands with the Fc. Transverse relaxation optimized spectroscopy (^{15}N-TROSY) NMR titration experiments are carried out using perdeuterated ^{15}N-labeled $F_C$with both single mode and MM CEX ligands in free solution to identify primary binding sites on the protein and to obtain residue specific binding affinities to the ligands. We then examine the NMR results as they compare to the protein surface property maps to develop a deeper understanding of the relation between the binding regions and patches on the protein surface. Finally, we employ MD simulations to provide further insights into the intermolecular interactions and binding mechanisms occurring with the F_C in MM systems.

Materials & Methods

Materials

Perdeuterated ^{15}N-labeled IgG1 $F_C$domain (residues 1-228 corresponding to residues 220-447 in the IgG1) expressed in *E. Coli* was provided by Merck & Co., Inc. (Kenilworth, NJ, 07033, USA). Disposable Zeba spin desalting columns (7K MWCO, 0.5 mL) were purchased from Thermo Fisher Scientific (Waltham, MA, 02451, USA). 1-propane sulfonic acid, 4-amino hippuric acid, sodium acetate, acetic acid, sodium azide and hydrochloric acid were purchased from Sigma-Aldrich (St. Louis, MO, 63103, USA). N-Benzoyl-dl-Methionine was purchased from Bachem Americas Inc. (Torrance, CA, 90505, USA). Capto MMC chromatographic resin was purchased from Cytiva (Uppsala, Sweden). Nuvia cPrime chromatographic resin was donated by Bio-Rad Laboratories (Hercules, CA, 94547, USA). Bruker^{TM}microbore NMR sample tubes were purchased from Norell (Morganton, NC, 28680, USA). D_2O was purchased from Cambridge Isotope Laboratories, Inc. (Tewksbury, MA, 01876, USA).

Chromatography Experiments

Chromatographic media were packed into a 5 x 50 mm column and experiments were carried out on an ÄKTA Explorer 100 (Cytiva, Upsella, Sweden) controlled by UNICORN 5.1 software. The IgG1 $F_C$domain was buffer-exchanged into buffer A (20 mM sodium acetate, pH 5) using Zeba spin desalting columns and diluted with buffer A to obtain a final protein concentration of 1 mg/mL. The chromatographic columns were equilibrated with buffer A followed by a 100 µL pulse injection of the buffer-exchanged F_C solution. Bound protein was eluted with a linear salt gradient from 100% buffer A to 100% buffer B (20 mM sodium acetate, 1 M NaCl, pH 5) over 40 column volumes (CV) at a flowrate of 1 CV/min. The column effluent was monitored at 280 nm. The average of the first moments from duplicate runs was used to determine the elution salt concentration.

Nuclear Magnetic Resonance Experiments

NMR spectra were obtained at 30°C using a Bruker 800-MHz NMR spectrometer equipped with a^{1}H/^{15}N/^{13}C cryoprobe with z-axis gradients. Data were acquired and processed using TopSpin 3.2 software and the Sparky 3 software package (Goddard and Kneller, University of California, San Francisco). Confirmation of the backbone assignments was guided using published chemical shift values (BMRB accession number 15514). Each sample had a constant protein concentration of 0.12 mM in the NMR buffer (10 mM sodium acetate, pH 5.0, 10% D_2O and 0.02% sodium azide). The ligands employed in the NMR experiments to represent the SP Sepharose, Capto MMC and Nuvia cPrime chromatographic resins are shown in Figure

1. A 1.0 M stock solution of the SP Sepharose ligand (1-propane sulfonic acid) was prepared in the NMR buffer. The Nuvia cPrime and Capto MMC ligands were available as lyophilized powders and were dissolved in 0.12 mM perdeuterated ^{15}N-labeled protein solution prior to titration. Due to the limited solubility of these ligands, the maximum solution concentration of Nuvia cPrime and Capto MMC ligands was 60 and 3.2 mM, respectively. Since the commercial material for Capto MMC is composed of immobilized enantiomers, a similar racemic mixture was used in these solution-based NMR experiments.

Ligand-induced changes in chemical shift were recorded in a series of^{15}N-TROSY experiments at a fixed $F_C$concentration (0.12 mM) and various F_C-ligand ratios (SP Sepharose, 1:1 to 1:800; Capto MMC, 1:0.5 to 1:25; and Nuvia cPrime, 1:0.5 to 1:320). Ligand-induced changes in chemical shift were in fast exchange and at a population- weighted average of the unbound and bound chemical shifts. The changes in combined chemical shift ([?]δ_{NH}) upon ligand addition were calculated using equation 1.

$$\delta_{\mathrm{NH}} = \sqrt{(\delta_H)^2 + (0.2 * \delta_N)^2} \quad (1)$$

where δ_H and δ_N represent the change in the chemical shift of the amide proton and nitrogen, respectively. A weighting factor of 0.2 was employed to account for the difference in sensitivity of proton and nitrogen chemical shifts of the amide group (Rule & Hitchens, 2005; Williamson, 2013). The binding dissociation constant (K_D) was calculated by fitting the changes in^{1}H and ^{15}N chemical shift as a function of ligand concentration using the single-site binding model (Rule & Hitchens, 2005) as described in equation 2.

$$\delta_{\mathrm{obs}} = \delta_u + \delta_b \frac{(K_D + [L]_T + [P]_T) - \sqrt{(K_D + [L]_T + [P]_T)^2 - (4 * [L]_T [P]_T)}}{2 * [P]_T} \quad (2)$$

where K_D is the apparent binding dissociation constant, $[L]_T$ and $[P]_T$ are the total ligand and protein concentrations used in the experiment and [?]δ_{obs} is the observed change in chemical shift upon ligand addition. [?]δ_u and [?]δ_b represent the changes in chemical shift for the unbound and bound states, respectively. Based on the K_D values and accounting for fitting error, residues that were interacting with the ligands were identified and clustered into binding sites. Curve fitting and calculations were performed on Matlab R2019b and the protein surface visualization was carried out on PyMol 2.3.5 viewer (Schrödinger).

Protein Surface Properties

A structural model for the IgG1 F_C domain was built by homology modeling starting with the crystal structure for an aglycosylated human IgG1 F_C fragment (PDB code: 3S7G) using Molecular Operating Environment (MOE 2018, Chemical Computing Group). The electrostatic potential (EP) maps were calculated using the adaptive Poisson-Boltzmann solver (APBS) (Baker, Sept, Joseph, Holst, & Andrew McCammon, 2001) and surface aggregation propensity (SAP) maps were calculated as described by Trout and co-workers (Chennamsetty, Voynov, Kayser, Helk, & Trout, 2010). The EP map was calculated at pH 5.0 to match the experimental conditions. The resulting protein surface maps were then visualized using the PyMol 2.0.6 viewer (Schrödinger).

Molecular Dynamics Simulations

MD simulations were performed with the two MM CEX ligands, Capto MMC and Nuvia cPrime in free solution around the F_C molecule, as shown in Figure 2. Each simulation was performed for 200ns with a timestep of 2fs and storing one frame every 1ps. The first 50ns were taken as equilibration time and all analyses were performed using the last 150ns. The simulation box dimensions were 8.5nm x 10nm x 13nm, allowing for a buffer of roughly 1.5nm on each side of the protein. The F_C was prevented from rotating in each simulation by restraining a single alpha carbon buried in the center of each of the four Fc domains using a

harmonic potential with a spring constant of 40,000kJ/mol/nm^2 (Srinivasan et al., 2017). This allowed the use of a rectangular simulation box without risking the protein interacting with itself through periodic boundary conditions. Additionally, each simulation contained sodium counterions for electroneutrality and an excess of 18 sodium and chloride such that there is a counterion for every charged side chain. A total of 61 ligands were included in each simulation, corresponding to a concentration of 0.1 M. The F_C was parameterized using the AMBER Parm99 (Cheatham, Cieplak, & Kollman, 1999) forcefield and PropKa (Bas, Rogers, & Jensen, 2008) was used to adjust the charge of the side chains to reflect a pH of 5.0. Water was modeled explicitly using the TIP3P (Jorgensen et al., 1981) water model and ligand atom types and nonbonded interactions were parameterized using the General AMBER Force Field (GAFF) (Wang, Wolf, Caldwell, Kollman, & Case, 2004). Atomic partial charges were obtained using a GAUSSIAN (Frisch, M.J.E.A., Trucks, G.W., Schlegel, H.B., Scuseria, G.E., Robb, M.A., Cheeseman, J.R., Scalmani, G., Barone, V., Mennucci, B., Petersson, 2009) calculation with RESP (Bayly, Cieplak, Cornell, & Kollman, 1993; Wang, Cieplak, & Kollman, 2000) assignment using the Antechamber tool of AMBER (Wang, Wang, Kollman, & Case, 2001), as has been described previously (Bilodeau, Lau, Cramer, & Garde, 2019). The resulting topologies were converted into the GROMACS format using ACPYPE (Silva & Vranken, 2012). In this work, partial negative charges on the carbons in the phenyl ring were employed rather than explicit parameterizations to reflect pi interactions.

Simulations were performed using GROMACS 4.5.3 (Hess, Kutzner, Van Der Spoel, & Lindahl, 2008; Pronk et al., 2013) in the NPT ensemble. The temperature and pressure were maintained at 298 K and 1 atm using a Nosé-Hoover thermostat (Evans & Holian, 1985) and a Parrinello-Rahman barostat (Parinello, M. and Rahman, 1980), respectively. Ligands, protein, and water/ions were treated as three separate temperature coupling groups. Electrostatic interactions were calculated using the Particle-Mesh Ewald (Darden, York, & Pedersen, 1993) method with a grid spacing of 0.1 nm, an order of 4 for the B-spline interpolation, and a direct sum tolerance of 10^{-5} (consistent with default parameters).

Results and Discussion

Chromatographic retention of the $F_C$domain

The linear salt gradient elution behavior of the IgG1 $F_C$domain was evaluated on a CEX resin (SP Sepharose) and two MM CEX systems (Capto MMC and Nuvia cPrime) and the resulting elution salt concentrations are presented in Figure 3. As can be seen, the F_C domain was weakly retained on the CEX resin, eluting at 0.12 M NaCl in the gradient. In contrast, the $F_C$domain exhibited significantly stronger retention on the two MM CEX systems with 0.63 and 0.9 M NaCl required for the elution from the Nuvia cPrime and Capto MMC resins, respectively. The higher retention on Capto MMC as compared to Nuvia cPrime could be due to the more solvent exposed aromatic moiety on the Capto ligand (Robinson, Roush, et al., 2018; J. Woo et al., 2015). Further, the elevated salt elution concentration seen in the MM resins as compared to the single mode CEX system is likely due to more complex interactions occurring with the $F_C$domain. In order to gain further insight into the interaction sites and binding mechanisms between these ligands and the F_C, TROSY titration experiments and MD simulations were carried out.

NMR Chemical Shift Perturbation Experiments

The binding of individual chromatographic ligands to the F_C in solution was evaluated using NMR spectroscopy with a perdeuterated ^{15}N-labeled F_C. The ligands employed to represent the SP Sepharose, Capto MMC and Nuvia cPrime resins are shown in Figure 1. As described in the Methods section, ligands were titrated against a fixed concentration of the labeled F_C and the binding was monitored via the resulting ^{15}N-TROSY spectra. In the NMR spectra, the amide groups on the ^{15}N-labeled amide backbone of the F_C that were in close proximity to ligands were observed to experience a change in the local electronic environment resulting in chemical shift perturbations (CSPs). In the resulting^{15}N-TROSY spectra, a single resonance

peak was observed for both the unbound and bound state of the protein for each amide group. Thus, the observed peak was a population weighted average of the two states and is defined by equation 3.

$$\delta_{\text{obs}} = f_u\delta_u + f_b\delta_b \quad (3)$$

where f_u and f_b are the fractions of the unbound and bound protein, respectively, and δ_u and δ_b are the chemical shift values of the unbound and bound states of the protein. The linewidths were largely free of exchange broadening and had ligand-dependent chemical shift values similar to those without ligands. This was indicative of 'fast-exchange' behavior for protein-ligand interactions. The changes in combined (^{1}H and ^{15}N) chemical shift ([?]δ_{NH}) were then calculated using equation 1.

An important first step towards binding analysis was to evaluate the CSPs for all the residues in the protein sequence. Accordingly, the plots of the observed CSPs at the highest concentrations of the SP Sepharose, Capto MMC and Nuvia cPrime ligands are presented in Figures 4a, b & c, respectively (note: the Fc residues 1-228 correspond to the IgG1 residues 220-447).The secondary structural elements of the F_C sequence are also shown at the bottom of Figure 4a. The data were analyzed using the statistical method described by Schumann et al. (Schumann et al., 2007) to determine the corrected standard deviation σ_0. The residues with CSPs smaller than σ_0 were grouped as non-interacting (noise) and are presented as grey bars in the Figures. Residues exhibiting large CSPs are represented in red bars while residues with intermediate changes are shown in a red-grey color gradient. As can be seen in Figure 4a, for interactions of the SP Sepharose ligand to the F_C, residues that experienced large changes in CSPs were spread across the entire protein sequence and did not group into a specific region. In addition, residues that exhibited intermediate changes were not localized around residues that showed large CSPs. In contrast to the single mode CEX ligand results, both the large and intermediate CSPs associated with the binding of MM CEX ligands were clearly clustered in specific regions in the F_C sequence (Figures 4b & c). Interestingly, the residues experiencing these CSPs were primarily located in clusters associated with more flexible regions of the protein. For example, by comparing these data with the secondary structural elements of the F_C, it can be seen that the clusters observed near residues 29-38 and 87-98 (Figures 4b & c) were associated with either loops or a combination of loops and α-helices. While the CSPs for the CEX and MM CEX systems were quite different, the changes within the MM CEX systems for Capto MMC and Nuvia cPrime were very similar. This was quantified by the Pearson correlation coefficient which was calculated to be 0.15 ± 0.03 for the CEX and each of the MM CEX systems and 0.85 for the Capto MMC and Nuvia cPrime systems (Figure S1).

To further visualize these ligand-induced changes in combined chemical shift, the CSPs for the residues were visualized on the protein surface using the PyMol viewer. A cartoon and a surface representation of these results for the three ligands studied are presented in Figures 5a and 6, respectively. To facilitate the discussion, the color schemes used in these figures are the same employed in Figure 4. As can be seen in Figure 5a, for interactions of the SP Sepharose ligand with the F_C, residues that exhibited large and intermediate CSPs were spread across the entire protein surface. Further, as expected for a cation exchange ligand such as SP Sepharose, the residues that experienced CSPs were often associated with positively charged (blue colored) regions on the electrostatic potential (EP) map of the F_C shown in Figure 5b.

In contrast, the results for binding of the Capto MMC and Nuvia cPrime ligands with the F_C, indicated a more focused interaction region as highlighted by the dotted blue ellipses of Figures 6a and b, respectively. Interestingly, the residues that interacted with the MM ligands and were present in the flexible loops and alpha helices (as discussed above for Figure 4) were located in the interface of the C_H2 and C_H3 domains. Further, residues that experienced ligand-induced CSPs were mostly identified to be positively charged and/or aliphatic or aromatic in nature. In order to examine this in more detail, the focused interaction region for the MM ligands was also indicated on the EP and SAP maps presented in Figure 5b and c. As can be seen in the figures, this region was associated with both positive EP and some hydrophobicity which is expected for the interactions of multimodal ligands (Karkov, Woo, Krogh, Ahmadian, & Cramer, 2015).

Interpretation of the CSP data does come with a few caveats. For example, residues that are in close

proximity of those directly interacting with the ligands may also undergo significant changes in chemical shift. In addition, residues interacting with a ligand may not experience significant changes in electronic environment and thus may not have a measurable CSP. In order to address these issues, the changes in combined chemical shift during the titration experiments were examined in more detail.

A few representative spectral overlays for the binding of the Nuvia cPrime ligand to F_C are presented in Figure 7 and the corresponding CSPs as a function of ligand concentration are shown in Figure S2. As can be seen in the figures, different trajectories of the CSPs were observed with increasing ligand concentration for each of the residues. For example, residue Asp 182 (Figures 7a and S2a) did not exhibit any significant shift with increasing ligand concentration, indicating that it likely did not participate in binding. For residues that did show measurable CSPs, we observed primarily linear migrations with both saturated and unsaturated behavior. As can be seen in Figures 7b and S2b, Val 178 exhibited linear migration without saturation, which could be due to non-specific and/or weak interactions of the ligand with this residue. On the other hand, for His 66 (Figures 7c & S2c), a saturating linear trajectory was observed which was indicative of a simple two-state binding behavior that could be readily fit to the Langmuir equation (equation 2) to determine the binding dissociation constant (K_D).

The CSP data at different ligand concentrations for all the F_C residues were fit to equation 2 using Matlab R2019b with a maximum fitting error of 10% in a 95% confidence interval. For interactions of the SP Sepharose ligand with the F_C, residues that showed saturation behavior exhibited high K_D values ($>$ 150 mM) which were indicative of very weak interactions. Further, the SP Sepharose ligand was observed to interact throughout the F_C surface without clustering into specific regions (results not shown).

Due to solubility constraints with the Capto MMC ligand ([?] 3.2 mM at pH 5), the K_D determination with the multimodal ligands was limited to the more soluble Nuvia cPrime ligand. The CSP data at different Nuvia cPrime ligand concentrations for all the F_C residues were fit to equation 2 to determine the residue specific K_D values which are presented in Table S1. Based on the maximum solubility of the Nuvia cPrime ligand (60 mM at pH 5), only K_D values below 40mM were able to be accurately determined. As can be seen in the Table, the resulting K_D values were up to two orders of magnitude smaller than those observed with the single mode SP Sepharose ligand. These results qualitatively agree with the marked differences observed in the elution salt concentrations, 0.12 and 0.63 M NaCl, for F_C in SP Sepharose and Nuvia cPrime chromatographic systems, respectively.

The F_C residues that exhibited saturation behavior for interactions with the Nuvia cPrime ligand were color coded based on their K_D values and the resulting projections on the protein surface are presented in Figure 8. As can be seen in the Figure, residues interacting with a "high" binding affinity (1.2 [?] K_D [?] 10 mM) were primarily located in the hinge region (green ellipse) and near the interface of the C_H2 and C_H3 domains (blue ellipse) (note: these regions are the same as those in Figure 6 which were based on the CSPs). The strong interactions with a cluster of positively charged (His 66, His 5, Lys 3 and Lys 55) and polar (Thr 4, Thr 6 and Cys 7) residues in the hinge region is indicative of this being a preferred binding region for the ligand. However, it is important to note that interactions observed near the flexible hinge region may be due to direct participation of the residues in ligand binding and/or NMR shifts due to ligand binding induced conformational changes in that region of the F_C. Further, while the hinge region was identified by NMR as a preferred binding region for the ligand, steric affects would likely impact ligand interactions with the F_C when present in an intact mAb and/or Fc fusion proteins.

As was observed with the CSP data (Figure 6), the $K_D$results also indicated that the interface of the C_H2 and C_H3 domains was an important preferred binding region for interacting with the Nuvia cPrime ligand (Figure 8). Residues involved in binding to the Nuvia cPrime ligand in this region are indicated in Table S1 with a #. As can be seen in the table, this contiguous MM ligand binding region was composed of positively charged (His 214, Arg 36, His 210 and His 91), polar (Asn 215, Gln 219, Thr 31, Thr 218, Thr 37, Gln 92, Ser 221, Ser 35 and Gly 166) and aliphatic (Leu 32, Ile 34, Ala 159, Val 160 and Met 33) residues. In this region, residue 214H interacted with one of the lowest K_D values (3.94 +- 2.1 mM), indicating relatively strong binding to the ligand. Interestingly, this histidine residue has also been shown to be one of the most

important residues for binding of the $F_C$portion of IgG1 mAbs to Protein A resins (Idusogie et al., 2000; Moiani et al., 2009). As can be seen in Table S1, a few negatively charged residues (e.g. Glu 211 and Asp 93) also exhibited NMR shifts which may be due to their proximity to the clusters of positively charged and polar residues discussed above.

As was discussed above with the CSP results, this preferred binding region at the interface of the C_H2 and C_H3 domains (indicated by the blue ellipse) corresponded to an overlapping region of positive EP and hydrophobicity (Figures 5b and c). The fact that the K_D results presented in Figure 8 are even more focused in this region lends further support to the importance of both types of interactions in MM systems.

Molecular Dynamics Simulations

The NMR experiments described so far provide a window into protein-multimodal ligand interactions on a molecular level. While NMR experiments yield molecularly-detailed data, they are time- and resource-intensive making it difficult to quickly apply these tools to a wide range of systems. In order to more deeply investigate the F_C-ligand interactions at the molecular level and to explore some of the docked conformations of the Nuvia cPrime ligands, we carried out MD simulations. As described in the Methods section, simulations were performed with multiple ligand copies in free solution with the protein, and throughout the simulation ligands were free to reversibly interact from the protein surface. The free energy of a ligand binding to a given region of the protein surface was calculated as:

$$G_{\text{binding}} = -k_B \text{T} \ln\left(\frac{\rho_{\text{bound}}}{\rho_{\text{bulk}}}\right) \quad (4)$$

where ρ_{bound} and ρ_{bulk} are the ligand density in the bound and bulk regions respectively, k_B is the Boltzmann constant and T is the temperature. The free energy was calculated at every grid point with 1Å spacing around the protein.

Figure 9 shows the free energy plotted on the surface of the F_C. As can be seen, the Nuvia cPrime ligands had a strong tendency to bind to the interface between the C_H2 and C_H3 regions as well as the hinge region. These hotspots are qualitatively consistent with those observed using NMR. Previous work in our group has shown that free ligand MD simulations can qualitatively predict hotspots observed in NMR experiments for small model proteins (Holstein, Chung, et al., 2012; Parimal et al., 2015). Here, we have shown for the first time that this is also true for large, therapeutically relevant proteins.

MD simulations are also valuable in that they can directly elucidate the mechanism of binding. To illustrate this, Figures 10a and b show example poses of Nuvia cPrime bound to the hinge region and the C_H2-C_H3 interface, respectively. In the hinge region (shown in Figure 10a) Nuvia cPrime interacts with a combination of histidines and hydrophobic methionines. Interestingly, the cluster of residues (Tyr 81, Lys 3, His 49 and Met 1) that were identified to interact with the Nuvia cPrime ligand are also a part of the natural complementary F_C binding sites for interactions with the C1q and FcRgIII receptors. In the C_H2-C_H3 interface (Figure 10b), ligands appeared to interact with the histidines through two mechanisms: direct positive (histidine)-negative (carboxylic acid) interactions, and pi-pi stacking (between the phenyl ring and histidine ring). Previous work in our group has shown that pH can be used as an effective tool for modulating the interactions of Fc with multimodal chromatographic supports (Robinson et al., 2020). The simulation results presented here suggest that this may be due to the strong ligand-histidine interactions, which would be significantly affected by a change in pH from 5 to 7.

Conclusions

In this paper, a combination of NMR and MD simulations was employed to develop a fundamental understanding of how single mode CEX and MM CEX chromatographic ligands interact with the F_C domain

of an IgG1 mAb. The NMR results provided insights into the interaction sites of these ligands on the F_C. Preliminary data analysis of the NMR results based on CSPs revealed that, while the single mode ligand interacted across the entire $F_C$surface, the MM ligands appeared to interact with specific clusters of residues forming a concentrated binding region. In order to obtain more quantitative information, the CSP data at different ligand concentrations for each F_C residue were fit to the Langmuir equation to determine the residue specific binding dissociation constants (K_D). While the single mode CEX ligand showed weak interactions over the F_C surface with high K_D values (> 150 mM), the Nuvia cPrime MM ligand exhibited up to two orders of magnitude smaller K_D values indicating significantly stronger binding to the F_C. The MM ligand binding sites on the F_C were concentrated in the hinge region and near the interface of the C_H2 and C_H3 domains which are relatively flexible regions of the F_C. These sites were also observed to consist of primarily positively charged, polar and aliphatic residues on the F_C surface. Interestingly, histidine residues in these regions exhibited some of the strongest binding to the MM ligand. Comparisons of the NMR results with protein surface properties suggested that the MM ligand binding regions were associated with overlapping regions of positive charge and hydrophobicity on the F_C surface. Finally, we presented MD simulations to provide further insights into the binding mechanisms these interactions. As was determined from the NMR analysis, the simulations also indicated that the histidine residues in the interface of the C_H2 and C_H3 domains were "high affinity" binders. The simulations also indicated that these histidines interacted with the MM ligands via electrostatic and pi-pi interactions.

This combined biophysical and simulations approach elucidates the MM ligand interaction sites on the F_C and sets the stage for future analyses of even more complex biotherapeutics such as Fabs and mAbs. While the current work was focused on only two MM ligands, this method can readily be extended to other MM ligands that have been recently shown to exhibit unique chromatographic selectivities for the separation of complex multi-domain proteins (Robinson, Roush, 2018). The molecular insights gained from this work can also potentially lead to new protein molecular descriptors that may be useful for predicting the multimodal chromatographic behavior of F_C containing molecules such as mAbs, bispecific Abs and fusion proteins. Future work will also examine the interactions of the Fc with MM ligand-coated nanoparticles in order to more fully account for co-operativity and avidity effects in these systems.

Acknowledgements

This work was supported by the National Science Foundation (Grant number CBET 1704745) as well as the ASC Graduate Fellowship Program from Lawrence Livermore National Laboratory, Merck & Co., Inc. (Kenilworth, NJ, 07033, USA).and Bio-Rad laboratories (Hercules, CA, 94547, USA). Work at the Lawrence Livermore National Laboratory (LLNL) was performed under the auspices of the U.S. Department of Energy by Lawrence Livermore National Laboratory under Contract DE-AC52-07NA27344.

References

Arakawa, T., Kita, Y., Sato, H., & Ejima, D. (2009). MEP chromatography of antibody and Fc-fusion protein using aqueous arginine solution.*Protein Expression and Purification* , *63* (2), 158–163. https://doi.org/10.1016/j.pep.2008.09.011

Baker, N. A., Sept, D., Joseph, S., Holst, M. J., & Andrew McCammon, J. (2001). *Electrostatics of nanosystems: Application to microtubules and the ribosome. Proceedings of the National Academy of Sciences, 98(18)* , 10037-10041. https://doi.org/10.1073/pnas.181342398.

Banerjee, S., Parimal, S., & Cramer, S. M. (2017). A molecular modeling based method to predict elution behavior and binding patches of proteins in multimodal chromatography. *Journal of Chromatography A ,1511* , 45–58. https://doi.org/10.1016/j.chroma.2017.06.059

Bas, D. C., Rogers, D. M., & Jensen, J. H. (2008). Very fast prediction and rationalization of pK a values for protein2ligand complexes.*Proteins* , *73* (3), 765–783. https://doi.org/10.1002/prot.22102

Bayly, C. I., Cieplak, P., Cornell, W. D., & Kollman, P. A. (1993).*A Well-Behaved Electrostatic Potential Based Method Using Charge Restraints for Deriving Atomic Charges: The RESP Model . The Journal of Physical Chemistry, 97,* 10269-10280.

Bilodeau, C. L., Lau, E. Y., Cramer, S. M., & Garde, S. (2019). Conformational Equilibria of Multimodal Chromatography Ligands in Water and Bound to Protein Surfaces. *Journal of Physical Chemistry B, 123,* 4833-4843. https://doi.org/10.1021/acs.jpcb.9b01218

Burton, S. C., Haggarty, N. W., & Harding, D. R. K. (1997). One step purification of chymosin by mixed mode chromatography.*Biotechnology and Bioengineering* , *56* (1), 45–55. https://doi.org/10.1002/(SICI)1097-0290(19971005)56:1<45::AID-BIT5>3.0.CO;2-V

Burton, Simon Christopher, & Harding, D. R. K. (1997). High-density ligand attachment to brominated allyl matrices and application to mixed mode chromatography of chymosin. *Journal of Chromatography A* ,*775* (1–2), 39–50. https://doi.org/10.1016/S0021-9673(97)00515-3

Cheatham, T. E., Cieplak, P., & Kollman, P. A. (1999). A Modified Version of the Cornell et al. Force Field with Improved Sugar Pucker Phases and Helical Repeat. *Journal of Biomolecular Structure and Dynamics* , *16* (4), 845–862. https://doi.org/10.1080/07391102.1999.10508297

Chen, J., Tetrault, J., Zhang, Y., Wasserman, A., Conley, G., DiLeo, M., ... Ley, A. (2010). The distinctive separation attributes of mixed-mode resins and their application in monoclonal antibody downstream purification process. *Journal of Chromatography A* ,*1217* (2), 216–224. https://doi.org/10.1016/J.CHROMA.2009.09.047

Chennamsetty, N., Voynov, V., Kayser, V., Helk, B., & Trout, B. L. (2010). Prediction of Aggregation Prone Regions of Therapeutic Proteins.*Journal of Physical Chemistry B, 114,* 6614–6624. https://doi.org/10.1021/jp911706q

Chung, W. K., Evans, S. T., Freed, A. S., Keba, J. J., Baer, Z. C., Rege, K., & Cramer, S. M. (2010). Utilization of lysozyme charge ladders to examine the effects of protein surface charge distribution on binding affinity in ion exchange systems. *Langmuir* , *26* (2), 759–768. https://doi.org/10.1021/la902135t

Chung, W. K., Freed, A. S., Holstein, M. A., Mccallum, S. A., Cramer, S. M., Designed, S. M. C., & Performed, M. A. H. (2010). Evaluation of protein adsorption and preferred binding regions in multimodal chromatography using NMR. *Proceedings of the National Academy of Sciences, 107(39)* , 16811–16816. https://doi.org/10.1073/pnas.1002347107

Chung, W. K., Holstein, M. A., Freed, A. S., Evans, S. T., Baer, Z. C., & Cramer, S. M. (2010). Ion exchange chromatographic behavior of a homologous cytochrome C variant library obtained by controlled succinylation. *Separation Science and Technology* , *45* (15), 2144–2152. https://doi.org/10.1080/01496395.2010.507432

Chung, W. K., Hou, Y., Holstein, M., Freed, A., Makhatadze, G. I., & Cramer, S. M. (2010). Investigation of Protein Binding Affinity and Preferred Orientations in Ion Exchange Systems Using a Homologous Protein Library. *Journal of Chromatography A* , *1217* (2), 191–198. https://doi.org/10.1016/j.chroma.2009.08.005

Clarkson, J., & Campbell, I. D. (2003). Studies of protein-ligand interactions by NMR. *Biochemical Society Transactions* ,*31* (Pt 5), 1006–1009. https://doi.org/10.1042/

Cramer, S. M., & Holstein, M. A. (2011). Downstream bioprocessing: recent advances and future promise. *Current Opinion in Chemical Engineering* , *1* , 27–37. https://doi.org/10.1016/j.coche.2011.08.008

Darden, T., York, D., & Pedersen, L. (1993). Particle mesh Ewald: An N⋅log(N) method for Ewald sums in large systems. *The Journal of Chemical Physics* , *98* , 5648. https://doi.org/10.1063/1.464397

Dismer, F., & Hubbuch, J. (2007). A novel approach to characterize the binding orientation of lysozyme on ion-exchange resins. *Journal of Chromatography A* , *1149* , 312–320. https://doi.org/10.1016/j.chroma.2007.03.074

Dismer, F., Petzold, M., & Hubbuch, J. (2008). Effects of ionic strength and mobile phase pH on the binding orientation of lysozyme on different ion-exchange adsorbents. *Journal of Chromatography A* ,*1194* (1), 11–21. https://doi.org/10.1016/J.CHROMA.2007.12.085

Evans, D. J., & Holian, B. L. (1985). The Nose-Hoover thermostat. *The Journal of Chemical Physics* , *83* (8), 4069–4074. https://doi.org/10.1063/1.449071

Freed, A. S., Garde, S., & Cramer, S. M. (2011). Molecular simulations of multimodal ligand-protein binding: Elucidation of binding sites and correlation with experiments. *Journal of Physical Chemistry B* ,*115* (45), 13320–13327. https://doi.org/10.1021/jp2038015

Frisch, M.J.E.A., Trucks, G.W., Schlegel, H.B., Scuseria, G.E., Robb, M.A., Cheeseman, J.R., Scalmani, G., Barone, V., Mennucci, B., Petersson, G. and N. (2009). Gaussian 09, Revision a. 02. *Gaussian. Inc., Wallingford, CT* , *200* . Retrieved from https://gaussian.com/g09citation/

Gagnon, P., Cheung, C.-W., Lepin, E. J., Wu, A. M., Sherman, M. A., Raubitschek, A. A., & Yazaki Pete Gagnon, P. J. (2010). *Minibodies and Multimodal Chromatography Methods: A Convergence of Challenge and Opportunity . Bioprocess International* 8(2), 26-35.

Gagnon, P., Cheung, C., & Yazaki, P. J. (2009). Cooperative multimodal retention of IgG , fragments , and aggregates on hydroxyapatite. *Journal of Separation Science, 32* , 3857–3865. https://doi.org/10.1002/jssc.200900055

Ghose, S., Hubbard, B., & Cramer, S. M. (2005). Protein interactions in hydrophobic charge induction chromatography (HCIC). *Biotechnology Progress* , *21* (2), 498–508. https://doi.org/10.1021/bp049712+

Hess, B., Kutzner, C., Van Der Spoel, D., & Lindahl, E. (2008). GROMACS 4: Algorithms for Highly Efficient, Load-Balanced, and Scalable Molecular Simulation. *Journal of Chemical Theory and Computation, 4,* 435-447. https://doi.org/10.1021/ct700301q

Holstein, M. A., Chung, W. K., Parimal, S., Freed, A. S., Barquera, B., McCallum, S. A., & Cramer, S. M. (2012). Probing multimodal ligand binding regions on ubiquitin using nuclear magnetic resonance, chromatography, and molecular dynamics simulations. *Journal of Chromatography A* , *1229* , 113–120. https://doi.org/10.1016/j.chroma.2011.12.101

Holstein, M. A., Parimal, S., McCallum, S. A., & Cramer, S. M. (2012). Mobile phase modifier effects in multimodal cation exchange chromatography. *Biotechnology and Bioengineering* , *109* (1), 176–186. https://doi.org/10.1002/bit.23318

Holstein, M. A., Parimal, S., McCallum, S. A., & Cramer, S. M. (2013). Effects of urea on selectivity and protein-ligand interactions in multimodal cation exchange chromatography. *Langmuir* ,*29* (1), 158–167. https://doi.org/10.1021/la302360b

Hong, Y.-H., Ahn, H.-C., Lim, J., Kim, H.-M., Ji, H.-Y., Lee, S., ... Lee, B.-J. (2009). Identification of a novel ubiquitin binding site of STAM1 VHS domain by NMR spectroscopy. *FEBS Letters* ,*583* (2), 287–292. https://doi.org/10.1016/j.febslet.2008.12.034

Idusogie, E. E., Presta, L. G., Totpal, K., Wong, P. Y., Meng, Y. G., & Mulkerrin, M. G. (2000). Mapping of the C1q Binding Site on Rituxan, a Chimeric Antibody with a Human IgG1 Fc. *Journal of Immunology* ,*164* , 4178–4184. https://doi.org/10.4049/jimmunol.164.8.4178

Johansson, B.-L., Belew, M., Eriksson, S., Glad, G., Lind, O., Maloisel, J.-L., & Norrman, N. (2003). Preparation and characterization of prototypes for multi-modal separation media aimed for capture of

negatively charged biomolecules at high salt conditions. *Journal of Chromatography A* , *1016* , 21–33. https://doi.org/10.1016/S0021-9673(03)01140-3

Jorgensen, W. L. (1981). Transferable Intermolecular Potential Functions for Water, Alcohols, and Ethers. Application to Liquid Water1.*Journal of American Chemical Society, 103,* 335-340.

Kaleas, K. A., Tripodi, M., Revelli, S., Sharma, V., & Pizarro, S. A. (2014). Evaluation of a multimodal resin for selective capture of CHO-derived monoclonal antibodies directly from harvested cell culture fluid. *Journal of Chromatography B* , *969* , 256–263. https://doi.org/10.1016/j.jchromb.2014.08.026

Karkov, H. S., Woo, J., Krogh, B. O., Ahmadian, H., & Cramer, S. M. (2015). Evaluation of selectivity in homologous multimodal chromatographic systems using in silico designed antibody fragment libraries. *Journal of Chromatography A* , *1426* , 102–109. https://doi.org/10.1016/j.chroma.2015.11.047

Kittelmann, J., Lang, K. M. H., Ottens, M., & Hubbuch, J. (2017). Orientation of monoclonal antibodies in ion-exchange chromatography: A predictive quantitative structure–activity relationship modeling approach. *Journal of Chromatography A* , *1510* , 33–39. https://doi.org/10.1016/j.chroma.2017.06.047

Lin, D.-Q., Tong, H.-F., Wang, H.-Y., & Yao, S.-J. (2012). Molecular Insight into the Ligand-IgG Interactions for 4-Mercaptoethyl-pyridine Based Hydrophobic Charge-Induction Chromatography. *Journal of Physical Chemistry B, 116,* 1393-1400. https://doi.org/10.1021/jp206817b

Liu, H. F., Ma, J., Winter, C., & Bayer, R. (2010). mAbs Recovery and purification process development for monoclonal antibody production.*MAbs* , *2* (5), 480–499. https://doi.org/10.4161/mabs.2.5.12645

Lu, R. C., Guo, X. R., Jin, C., & Xiao, J. X. (2009). NMR studies on binding sites and aggregation-disassociation of fluorinated surfactant sodium perfluorooctanoate on protein ubiquitin. *Biochimica et Biophysica Acta - General Subjects* , *1790* (2), 134–140. https://doi.org/10.1016/j.bbagen.2008.10.009

Melander, W. R., El Rassi, Z., & Horvath, C. (1989). Interplay of hydrophobic and electrostatic interactions in biopolymer chromatography : Effect of salts on the retention of proteins.*Journal of Chromatography A* , *469* , 3–27. https://doi.org/10.1016/S0021-9673(01)96437-4

Moiani, D., Salvalaglio, M., Cavallotti, C., Bujacz, A., Redzynia, I., Bujacz, G., ... Fassina, G. (2009). Structural Characterization of a Protein A Mimetic Peptide Dendrimer Bound to Human IgG. *Journal of Physical Chemistry B* , *113* (50), 16268–16275. https://doi.org/10.1021/jp909405b

O'Connor, E., Aspelund, M., Bartnik, F., Berge, M., Coughlin, K., Kambarami, M., ... Wang, W. (2017). Monoclonal antibody fragment removal mediated by mixed mode resins. *Journal of Chromatography A* , *1499* , 65–77. https://doi.org/10.1016/j.chroma.2017.03.063

Parimal, S., Garde, S., & Cramer, S. M. (2015). Interactions of Multimodal Ligands with Proteins: Insights into Selectivity Using Molecular Dynamics Simulations. *Langmuir, 31,* 7512-7523. https://doi.org/10.1021/acs.langmuir.5b00236

Parimal, S., Garde, S., & Cramer, S. M. (2017). Effect of guanidine and arginine on protein–ligand interactions in multimodal cation-exchange chromatography. *Biotechnology Progress* , *33* (2), 435–447. https://doi.org/10.1002/btpr.2419

Parinello, M. and Rahman, A. (1980). Crystal Structure and Pair Potentials: A Molecular-Dynamics Study, *The American Physical Society, 45(14),* 1–22.

Pezzini, J., Joucla, G., Gantier, R., Toueille, M., Lomenech, A. M., Le Senechal, C., ... Cabanne, C. (2011). Antibody capture by mixed-mode chromatography: A comprehensive study from determination of optimal purification conditions to identification of contaminating host cell proteins. *Journal of Chromatography A* , *1218* (45), 8197–8208. https://doi.org/10.1016/j.chroma.2011.09.036

Pronk, S., Pall, S., Schulz, R., Larsson, P., Bjelkmar, P., Apostolov, R., ... Lindahl, E. (2013). GROMACS 4.5: A high-throughput and highly parallel open source molecular simulation toolkit.*Bioinformatics* , *29* (7),

845–854. https://doi.org/10.1093/bioinformatics/btt055

Robinson, J., Roush, D., & Cramer, S. (2018). Domain contributions to antibody retention in multimodal chromatography systems. *Journal of Chromatography A* , *1563* , 89–98. https://doi.org/10.1016/j.chroma.2018.05.058

Robinson, J., Roush, D., & Cramer, S. M. (2020). The effect of pH on antibody retention in multimodal cation exchange chromatographic systems. *Journal of Chromatography A* , *1617* , 460838. https://doi.org/10.1016/j.chroma.2019.460838

Robinson, J., Snyder, M. A., Belisle, C., Liao, J., Chen, H., He, X., ... Cramer, S. M. (2018). Investigating the impact of aromatic ring substitutions on selectivity for a multimodal anion exchange prototype library. *Journal of Chromatography A* , *1569* , 101–109. https://doi.org/10.1016/J.CHROMA.2018.07.049

Roush, D. J., Gill, D. S., & Willson, R. C. (1994). *Electrostatic Potentials and Electrostatic Interaction Energies of Rat Cytochrome b5 and a Simulated Anion-Exchange Adsorbent Surface. Biophysical Journal, 66,* 1290-1300. https://doi.org/10.1016/S0006-3495(94)80924-5

Rule, G. S., & Hitchens, T. K. (2005). *Fundamentals of protein NMR spectroscopy* . Dordrecht, Netherlands: Springer.

Schumann, F. H., Hubert, A. E., Ae, R., Maurer, T., Wolfram, A. E., Ae, G., ... Kalbitzer, R. (2007). Combined chemical shift changes and amino acid specific chemical shift mapping of protein-protein interactions. *Journal of Biomolecular NMR* , *39* , 275–289. https://doi.org/10.1007/s10858-007-9197-z

Shukla, A. A., Hubbard, B., Tressel, T., Guhan, S., & Low, D. (2007). Downstream processing of monoclonal antibodies-Application of platform approaches. *Journal of Chromatography B* , *848* , 28–39. https://doi.org/10.1016/j.jchromb.2006.09.026

Silva, D., & Vranken, B. F. (2012). *ACPYPE-AnteChamber PYthon Parser interfacE . BMC Research Notes, 5,* 1-8.

Srinivasan, K., Banerjee, S., Parimal, S., Sejergaard, L., Berkovich, R., Barquera, B., ... Cramer, S. M. (2017). Single Molecule Force Spectroscopy and Molecular Dynamics Simulations as a Combined Platform for Probing Protein Face-Specific Binding. *Langmuir* , *33* , 10851-10860. https://doi.org/10.1021/acs.langmuir.7b03011

Srinivasan, K., Parimal, S., Lopez, M. M., McCallum, S. A., & Cramer, S. M. (2014). Investigation into the molecular and thermodynamic basis of protein interactions in multimodal chromatography using functionalized nanoparticles. *Langmuir* , *30* (44), 13205–13216. https://doi.org/10.1021/la502141q

Sun, Y., Welsh, W. J., & Latour, R. A. (2005). Prediction of the Orientations of Adsorbed Protein Using an Empirical Energy Function with Implicit Solvation. *Langmuir, 21,* 5616-5626. https://doi.org/10.1021/la046932o

Wang, J., Cieplak, P., & Kollman, P. A. (2000). How Well Does a Restrained Electrostatic Potential (RESP) Model Perform in Calculating Conformational Energies of Organic and Biological Molecules? *Journal of Computational Chemistry* , *21* (12), 1049–1074. https://doi.org/10.1002/1096-987X(200009)21:12<1049::AID-JCC3>3.0.CO;2-F

Wang, J., Wang, W., Kollman, P. A., & Case, D. A. (2001). *Antechamber, An Accessory Software Package For Molecular Mechanical Calculations. Journal of American Chemical Society, 222,* 41.

Wang, J., Wolf, R. M., Caldwell, J. W., Kollman, P. A., & Case, D. A. (2004). Development and testing of a general Amber force field. *Journal of Computational Chemistry* , *25* (9), 1157–1174. https://doi.org/10.1002/jcc.20035

Williamson, M. P. (2013). Progress in Nuclear Magnetic Resonance Spectroscopy Using chemical shift perturbation to characterise ligand binding. *Progress in Nuclear Magnetic Resonance Spectroscopy* ,*73* ,

1–16. https://doi.org/10.1016/j.pnmrs.2013.02.001

Woo, J. A., Chen, H., Snyder, M. A., Chai, Y., Frost, R. G., & Cramer, S. M. (2015). Defining the property space for chromatographic ligands from a homologous series of mixed-mode ligands. *Journal of Chromatography A* , *1407* , 58–68. https://doi.org/10.1016/j.chroma.2015.06.017

Woo, J., Parimal, S., Brown, M. R., Heden, R., & Cramer, S. M. (2015). The effect of geometrical presentation of multimodal cation-exchange ligands on selective recognition of hydrophobic regions on protein surfaces. *Journal of Chromatography A* , *1412* , 33–42. https://doi.org/10.1016/j.chroma.2015.07.072

Yao, Y., & Lenhoff, A. M. (2004). Electrostatic Contributions to Protein Retention in Ion-Exchange Chromatography. 1. Cytochrome c Variants. *Analytical Chemistry* , *59* (3), 6743. https://doi.org/10.1021/ac049327z

Yu, G., Liu, J., & Zhou, J. (2015). Mesoscopic Coarse-Grained Simulations of Hydrophobic Charge Induction Chromatography (HCIC) for Protein Purification. *AIChE Journal* , *61* (6), 2035–2047. https://doi.org/10.1002/aic

Zhang, L., Zhao, G., & Sun, Y. (2009). Molecular Insight into Protein Conformational Transition in Hydrophobic Charge Induction Chromatography: A Molecular Dynamics Simulation. *J. Phys. Chem. B* , *113* , 6873–6880. https://doi.org/10.1021/jp809754k

Figure Legends

Figure 1: The Ligands employed in NMR experiments to represent the chromatographic resins; (a) SP Sepharose, (b) Nuvia cPrime and (c) Capto MMC ligands.

Figure 2: Snapshot from MD simulation of F_C surrounded by Capto MMC ligands in free solution. Protein is shown in a surface representation in grey, water is shown in wireframe and colored based on atom type, and ligands and ions are shown in a licorice representation and colored based on atom type. Color scheme: hydrogen, white; oxygen, red; carbon, cyan; nitrogen, blue; and sulfur, yellow.

Figure 3: Chromatographic Retention of the F_C domain on single mode SP Sepharose and MM CEX systems. 40 CV linear salt gradient from 0 to 1M NaCl at pH 5.

Figure 4: Residue specific ligand-induced changes in combined chemical shift for binding of (a) SP Sepharose, (b) Capto MMC and (c) Nuvia cPrime ligands to the F_C domain. Secondary structure of the F_C domain at the bottom of a. Numbered regions 2-14; 25-38; 61-70; 87-98; 119-127; 154-157; 211-216; represent the loops & α-helices. (Note: different y-axis scale for Nuvia cPrime).

Figure 5: (a) A colored cartoon and surface representation of residue specific ligand induced changes in combined chemical shift upon binding of SP Sepharose ligand to the F_C domain. (b) Electrostatic Potential (EP) map at pH 5 and (c) Surface Aggregation Propensity (SAP) map of the F_C domain. (Note: numbered regions 1-13; 25-38; 87-98; 119-127; 211-216; represent the loops & α-helices).

Figure 6: A colored cartoon and surface representation of residue specific ligand induced changes in chemical shift for binding of (a) Capto MMC and (b) Nuvia cPrime ligands to the F_C domain. (Note: numbered regions 1-13; 25-38; 87-98; 119-127; 211-216; represent the loops & α-helices).

Figure 7: Representative ^{15}N-TROSY peaks from the Nuvia cPrime titration experiments for residues (a) Aspartate 182, (b) Valine 178 and (c) Histidine 66 at 0 (purple), 5 (magenta), 10(cyan), 20 (green), 40 (pink) mM ligand concentrations

Figure 8: Nuvia cPrime binding sites on F_C domain as determined by NMR with color coded dissociation constant (K_D) for non-interacting, grey; and strong, red; intermediate, salmon; and weak, pink; binding residues. Residues located in the hinge and C_H2-C_H3 interface regions are highlighted in green and blue ellipses, respectively.

Figure 9: Nuvia cPrime binding hotspots on the F_C as determined by MD simulations.

Figure 10: The dual role of protonated histidines in the (a) flexible hinge region and (b) interface of the C_H2 and C_H3 domains.

Figure S1: Comparison of the CSP data between (a) Nuvia cPrime and SP Sepharose, blue; (b) Capto MMC and SP Sepharose, brown; and (c) Capto MMC and Nuvia cPrime, purple; ligand systems.

Figure S2: Representative ligand induced changes in chemical shift as a function of Nuvia cPrime ligand concentration and the resulting fits for residues (a) Aspartate 182, (b) Valine 178 and (c) Histidine 66.

Table S1: A List of residues on the F_C surface interacting with Nuvia cPrime ligand, associated binding dissociation constant (K_D) with the standard error of fitting and the coefficient of determination (R^2). Residues located in the hinge and C_H2-C_H3 interface regions are indicated by * and #, respectively.

Figure 1: The Ligands employed in NMR experiments to represent the chromatographic resins; (a) SP Sepharose, (b) Nuvia cPrime and (c) Capto MMC ligands.

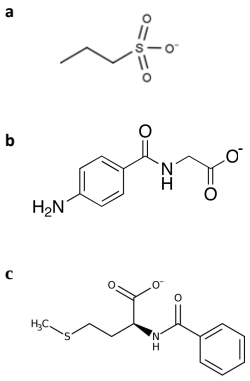

Hosted file

`Free ligand NMR paper figures.pdf` available at https://authorea.com/users/347444/articles/473120-identification-of-preferred-multimodal-ligand-binding-regions-on-igg1-fc-using-nuclear-magnetic-resonance-and-molecular-dynamics-simulations